

# Hollow multilayer photonic bandgap fibers for NIR applications

Ken Kuriki, Ofer Shapira, Shandon D. Hart, Gilles Benoit, Yuka Kuriki, Jean F Viens, Mehmet Bayindir, John D. Joannopoulos and Yoel Fink

Research Laboratory of Electronics and Department of Materials Science and Engineering, Massachusetts Institute of Technology, Cambridge, Massachusetts, 02139, USA  
[yoel@mit.edu](mailto:yoel@mit.edu)

<http://mit-pbg.mit.edu/>

**Abstract:** Here we report the fabrication of hollow-core cylindrical photonic bandgap fibers with fundamental photonic bandgaps at near-infrared wavelengths, from 0.85 to 2.28  $\mu\text{m}$ . In these fibers the photonic bandgaps are created by an all-solid multilayer composite meso-structure having a photonic crystal lattice period as small as 260 nm, individual layers below 75 nm and as many as 35 periods. These represent, to the best of our knowledge, the smallest period lengths and highest period counts reported to date for hollow PBG fibers. The fibers are drawn from a multilayer preform into extended lengths of fiber. Light is guided in the fibers through a large hollow core that is lined with an interior omnidirectional dielectric mirror. We extend the range of materials that can be used in these fibers to include poly(ether imide) (PEI) in addition to the arsenic triselenide ( $\text{As}_2\text{Se}_3$ ) glass and poly(ether sulfone) (PES) that have been used previously. Further, we characterize the refractive indices of these materials over a broad wavelength range (0.25 – 15  $\mu\text{m}$ ) and incorporated the measured optical properties into calculations of the fiber photonic band structure and a preliminary loss analysis.

©2004 Optical Society of America

**OCIS codes:** (060.2280) Fiber design and fabrication, (230.4170) Multilayers, (160.4670) Optical materials

---

## References and links

1. R. F. Cregan, B. J. Mangan, J. C. Knight, T. A. Birks, P. St. J. Russell, P. J. Roberts, D. C. Allan, "Single-mode photonic band gap guidance of light in air," *Science* **285**, 1537-1539 (1999).
2. D. C. Allan, J. A. West, J. C. Fajardo, M. T. Gallagher, K. W. Koch, and N. F. Borrelli, "Photonic crystal fibers: effective-index and bandgap guidance," in *Photonic Crystals and Light Localization in the 21st Century*, C. M. Soukoulis, ed (Kluwer, 2001).
3. B. J. Eggleton, C. Kerbage, P. S. Westbrook, R. S. Windeler, and A. Hale, "Microstructured optical fiber devices," *Opt. Express* **9**, 698-713 (2001), <http://www.opticsexpress.org/abstract.cfm?URI=OPEX-9-13-698>.
4. P. Yeh, A. Yariv, and E. Marom, "Theory of bragg fiber," *J. Opt. Soc* **68**, 1196-1201 (1978).
5. C. M. Smith, N. Venkataraman, M. T. Gallagher, D. Muller, J. A. West, N. F. Borrelli, D. C. Allan and K. W. Koch, "Low-loss hollow-core silica/air photonic bandgap fibre," *Nature* **424**, 657-659 (2003).
6. G. Bouwamans, F. Laun, J. C. Knight, P. St. J. Russell, L. Farr, B. J. Mangan, and H. Sabert, "Properties of a hollow-core photonic bandgap fiber at 850 nm wavelength," *Opt. Express* **11**, 1613-1620 (2003), <http://www.opticsexpress.org/abstract.cfm?URI=OPEX-11-14-1613>.
7. D. G. Ouzounov, F. R. Ahmad, D. Muller, N. Venkataraman, M. T. Gallagher, M. G. Thomas, J. Silcox, K. W. Koch, and A. L. Gaeta, "Generation of megawatt optical solitons in hollow-core photonic band-gap fibers," *Science* **301**, 1702-1704 (2003).
8. F. Benadid, J. C. Knight, G. Antonopoulos, P. St. J. Russell, "Stimulated raman scattering in hydrogen-filled hollow-core photonic crystal fiber," *Science* **298**, 399-402 (2002).
9. B. Temelkuran, S. D. Hart, G. Benoit, J. D. Joannopoulos and Y. Fink, "Wavelength-scalable hollow optical fibres with large photonic bandgaps for CO<sub>2</sub> laser transmission," *Nature* **420**, 650-653 (2002).

10. M. Ibanescu, Y. Fink, S. Fan, E. L. Thomas, and J. D. Joannopoulos, "An all-dielectric coaxial waveguide," *Science* **289**, 415-419 (2000).
11. S. G. Johnson, M. Ibanescu, M. Skorobogatiy, O. Weisberg, T. D. Engeness, M. Soljacic, S. A. Jacobs, J. D. Joannopoulos, and Y. Fink "Low-loss asymptotically single-mode propagation in large-core OmniGuide fibers," *Opt. Express* **9**, 748-779 (2001), <http://www.opticsexpress.org/abstract.cfm?URI=OPEX-9-13-748>.
12. Y. Fink, D.J. Ripin, S. Fan, C. Chen, J.D. Joannopoulos, E.L. Thomas, "Guiding optical light in air using an all-dielectric structure," *J. Lightwave Technol.* **17**, 2039-2041 (1999).
13. M. Soljacic, M. Ibanescu, S. G. Johnson, J. D. Joannopoulos, and Y. Fink, "Optical bistability in axially modulated OmniGuide fibers," *Opt. Lett.* **28**, 516-518 (2003).
14. T. D. Engeness, M. Ibanescu, S. G. Johnson, O. Weisberg, M. Skorobogatiy, S. Jacobs, and Y. Fink, "Dispersion tailoring and compensation by modal interactions in OmniGuide fibers," *Opt. Express* **11**, 1175-1198 (2003), <http://www.opticsexpress.org/abstract.cfm?URI=OPEX-11-10-1175>.
15. Y. Fink, J. N. Winn, S. Fan, C. Chen, J. Michel, J. D. Joannopoulos, and E. L. Thomas, "A dielectric omnidirectional reflector," *Science* **282**, 1679-1682 (1998).
16. S. D. Hart, G. R. Maskaly, B. Temelkuran, P. H. Pridaux, J. D. Joannopoulos, and Y. Fink, "External Reflection from omnidirectional dielectric mirror fibers," *Science* **296**, 510-513 (2002).
17. M. Ibanescu, S. G. Johnson, M. Soljacic, J. D. Joannopoulos, Y. Fink, O. Weisberg, T. D. Engeness, S. A. Jacobs, and M. Skorobogatiy, "Analysis of mode structure in hollow dielectric waveguide fibers," *Phys. Rev. E* **67**, 046608-1-8, (2003).
18. G. Benoit and Y. Fink, Spectroscopic Ellipsometry Database, <http://mit-pbg.mit.edu/Pages/Ellipsometry.html>
19. J. D. Joannopoulos, R.D. Meade, and J.N. Winn, "Photonic crystals: molding the flow of light", (Princeton University Press, Princeton, New Jersey, 1995).

## 1. Introduction

Hollow-core photonic bandgap fibers have been made from arrays of air holes in a solid dielectric [1-3] and from pairs of solid materials forming multilayer structures (also called Bragg fibers) [4]. Recently, researchers have reported on hollow-core photonic bandgap fibers with low losses around 1.5  $\mu\text{m}$  [5] and 850 nm [6] based on silica-air 2-D photonic crystal structures. In addition, researchers have made use of the tailorable dispersion and nonlinear characteristics of these fibers to demonstrate novel effects in ultrafast pulse propagation and the nonlinear optics of gases [7,8].

Here we report on multilayer photonic bandgap fibers that confine light in a hollow core [4]. These fibers have an all-solid meso-scale structure consisting of multiple alternating layers of high- and low-index materials surrounding a cylindrical hollow core. Hollow core guiding versions of these fibers have recently been successfully fabricated, with fundamental photonic bandgaps at 3 and 10.6  $\mu\text{m}$  wavelength [9]. While those wavelengths may be used for high-energy laser delivery, it is also of interest to explore the usage of these fibers at near-infrared (IR) wavelengths where most modern solid-state lasers operate, enabling applications ranging from standard telecommunications to ultrafast physics. In particular, those fibers that have a large refractive index contrast between the layer materials have been shown theoretically to allow great reductions in fiber losses and non-linearities as well as widely tunable dispersion and other interesting properties [10-14]. The high refractive index contrast between the layer materials leads to large photonic bandgaps and makes the inner lining of the fiber analogous to an omnidirectional dielectric mirror [15,16]. This structure should therefore have short electromagnetic penetration depths within the layer structure, minimizing the interaction of light with the layer materials [17]. Here we report for the first time the fabrication of hollow-core guiding cylindrical photonic bandgap fibers at near-IR wavelengths, from 0.85 to 2.28  $\mu\text{m}$ . These fibers require a significant reduction in feature size from previous work; the photonic crystal lattice periods in the fibers fabricated were drawn down to 260 nm.

To-date, structured fibers in general have been produced using a fairly narrow range of materials which limit the range of applications. An important focus of our research has been the identification of pairs of thermo-mechanically solid materials which can be assembled into a preform and co-drawn into fibers. The full set of necessary materials-compatibility conditions has not been completely established it is apparent though, that the ability to achieve small feature sizes while maintaining geometry depends on the material's viscosities at the drawing temperature and surface energies. In this work we introduce a new material,

poly(ether imide) (PEI) into the layered structure of these fibers, combined with the arsenic triselenide ( $\text{As}_2\text{Se}_3$ ) and poly(ether sulfone) (PES) that have been used in the past. We have also performed broadband (0.4-15  $\mu\text{m}$ ) spectroscopic ellipsometry measurements on PEI, PES, and  $\text{As}_2\text{Se}_3$  and incorporated the resulting experimentally determined real and imaginary refractive index values into photonic band diagram calculations for PEI and  $\text{As}_2\text{Se}_3$ , and for fiber loss calculations.

## 2. Experimental

Refractive indices of  $\text{As}_2\text{Se}_3$ , PEI and PES were measured using a SOPRA broadband spectroscopic ellipsometer.  $\text{As}_2\text{Se}_3$  films were prepared by thermal evaporation onto a silicon substrate. PEI and PES were prepared by spin coating from polymer solutions onto silicon substrates. The nominally stoichiometric composition of the evaporated  $\text{As}_2\text{Se}_3$  films was verified by electron microprobe analysis. The  $\text{As}_2\text{Se}_3$  films were confirmed to be amorphous both before and after fiber drawing using Raman microprobe spectroscopy.

The fiber preform was fabricated by the thermal evaporation of an  $\text{As}_2\text{Se}_3$  layer (2-5  $\mu\text{m}$ ) on each side of a free-standing 9-15- $\mu\text{m}$ -thick PEI film, and the subsequent 'rolling' of that coated film into a hollow multilayer tube. This hollow macroscopic preform was consolidated by heating under vacuum, and clad with a thick outer layer of PES; the layered preform was then placed in an optical fiber draw tower, and drawn down into hundreds of meters of fiber having well controlled submicrometer layer thicknesses and photonic bandgaps in the near-IR. The final layer thicknesses of the semiconducting  $\text{As}_2\text{Se}_3$  layers were as small as 60 nm. The spectral positions of the photonic bandgaps were controlled by the optical monitoring of the outer diameter of the fibers during draw. Typical standard deviations in the fiber outer diameter were ~1-2% of that diameter.

Fiber transmission spectra in the near to mid-IR were measured with a Fourier-transform infrared (FTIR) spectrometer (Bruker Optics Tensor 37), using a lens to couple light into the fiber and an external detector.

## 3. Results and discussion

Scanning electron microscope (SEM) imaging (Fig. 1) of a hollow-core cylindrical bandgap fiber with a fundamental bandgap of 2.28  $\mu\text{m}$  reveals that the drawn fiber maintains proportional layer thickness ratios, and that the PEI and  $\text{As}_2\text{Se}_3$  films maintain their structure during rigorous thermal cycling and elongation.

The real and imaginary components of the refractive indices of PEI, PES, and  $\text{As}_2\text{Se}_3$  from 0.25 to 15  $\mu\text{m}$  wavelength are compared in Fig. 2. [18]. The polymeric materials have significant vibrational absorption bands from 5  $\mu\text{m}$  to 15  $\mu\text{m}$ , resulting in sharp index variations. The  $\text{As}_2\text{Se}_3$  has a large, smooth change in refractive index between 400 and 800 nm due to its electronic bandgap around 1.83 eV. The Fig. 2 inset magnifies the wavelength region from 0.4 to 2  $\mu\text{m}$ . At 1.55  $\mu\text{m}$ , the refractive indices of PEI, PES, and  $\text{As}_2\text{Se}_3$  are 1.66, 1.62, and 2.82, respectively. These results for the real and imaginary index measurements were used for the calculation of the photonic band diagram shown in Fig. 3 as well as for the estimation of the fiber losses via leaky mode loss analysis. While good agreement was obtained for the location of the fundamental and higher order bandgaps, loss estimation for a non-ideal fiber is more complex. A brief discussion on fiber losses is given below, but a full analysis is reserved for a future paper dedicated to studying loss mechanisms in 1-D photonic crystal fibers.

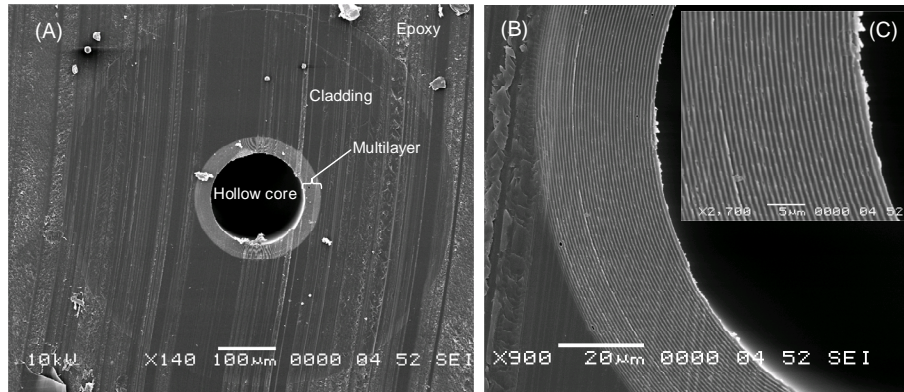


Fig. 1. Cross-sectional SEM micrographs of a 684- $\mu\text{m}$ -OD fiber with a fundamental photonic bandgap at a wavelength of 2.28  $\mu\text{m}$  mounted in epoxy are shown in (A), with multilayer structure lining around hollow core; (B) demonstrates the integrity of the multilayer structure; (C) reveals the ordering of alternating layers with  $\text{As}_2\text{Se}_3$  (bright layers), and PEI (grey layers). The PEI layers have a thickness of 470 nm, and the  $\text{As}_2\text{Se}_3$  layers are 270-nm-thick.

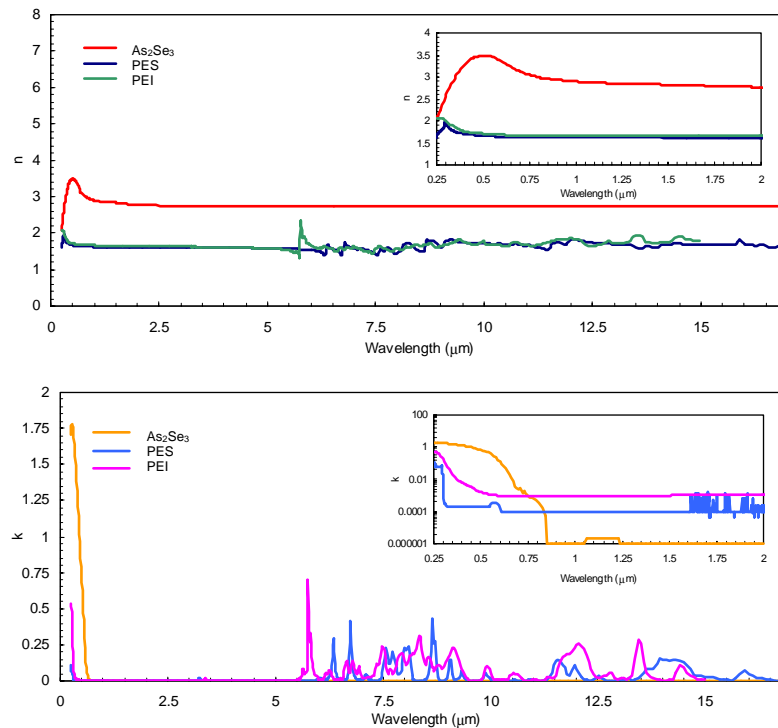


Fig. 2. Real ( $n$ , upper panel) and imaginary ( $k$ , lower panel) refractive indices of  $\text{As}_2\text{Se}_3$ , PEI and PES measured by spectroscopic ellipsometry from 0.25 to 15  $\mu\text{m}$  wavelength. The insets magnify the region between 0.25 and 2  $\mu\text{m}$  (with  $k$  on logarithmic scale). The polymeric materials have vibrational absorption modes from 5  $\mu\text{m}$  to 15  $\mu\text{m}$ , while  $\text{As}_2\text{Se}_3$  has an absorption band below 680 nm due to its electronic bandgap.

The upper panel of Fig. 3 shows the photonic band diagram for an  $\text{As}_2\text{Se}_3$  / PEI multilayer mirror calculated using Bloch wave / eigenvalue techniques (assuming an infinite periodic multilayer structure) [19]. This diagram was calculated using the measured indices of the fiber materials. Nominal layers ratio and bilayer thickness were determined using SEM imaging (Fig.1). The measured transmission spectrum for a hollow-core photonic bandgap fiber is shown in the lower panel of Fig. 3, using a 5-cm-long fiber with FTIR spectroscopy. The fundamental photonic bandgap is centered around  $2.28 \mu\text{m}$ , and the second and the third-order gaps are at  $1.14 \mu\text{m}$  and  $0.8 \mu\text{m}$ , respectively. The good agreement between the measured transmission spectrum and the band diagram strongly indicates that transmission through the fiber is dominated by the photonic bandgap mechanism.

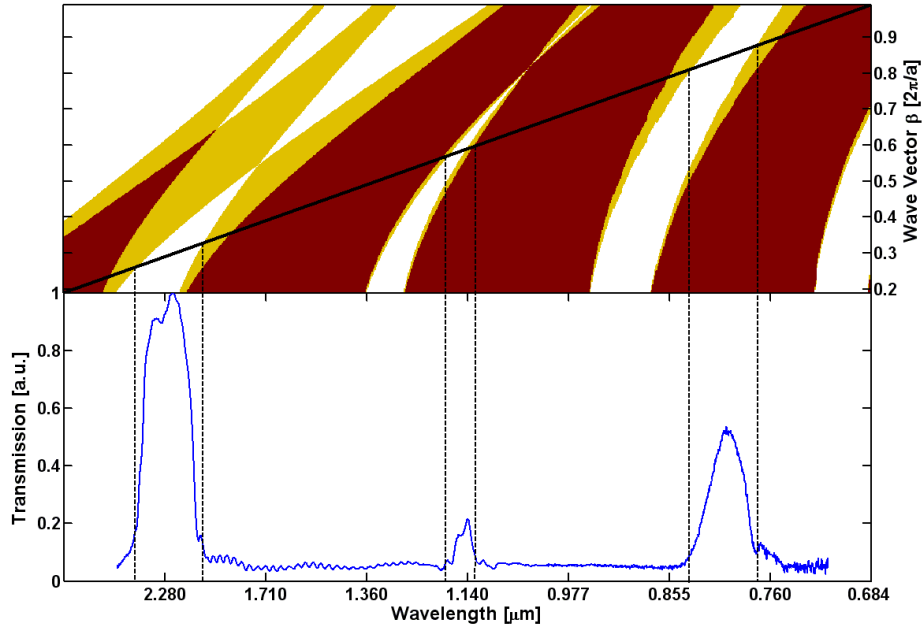


Fig. 3. Lower panel – FTIR spectrum measurement for a hollow-core photonic bandgap fiber. The fundamental photonic bandgap is centered around  $2.28 \mu\text{m}$ . The second and the third-order gaps are at  $1.14 \mu\text{m}$  and  $0.8 \mu\text{m}$ , respectively. Upper panel - Calculated photonic band diagram for a one dimensional photonic crystal made of alternating layers of  $\text{As}_2\text{Se}_3$  and PEI. The dark red and beige regions represent modes radiating thorough the multilayer structures for both the TE and TM modes, and only TM, respectively. Modes propagating through air and reflected by the fiber walls lie in the bandgaps (white) and within the light cone defined by the glancing-angle condition (black line). Pure TE modes can be confined more than pure TM modes. Refractive indices used in this calculation were experimentally obtained from ellipsometry (Fig. 2).

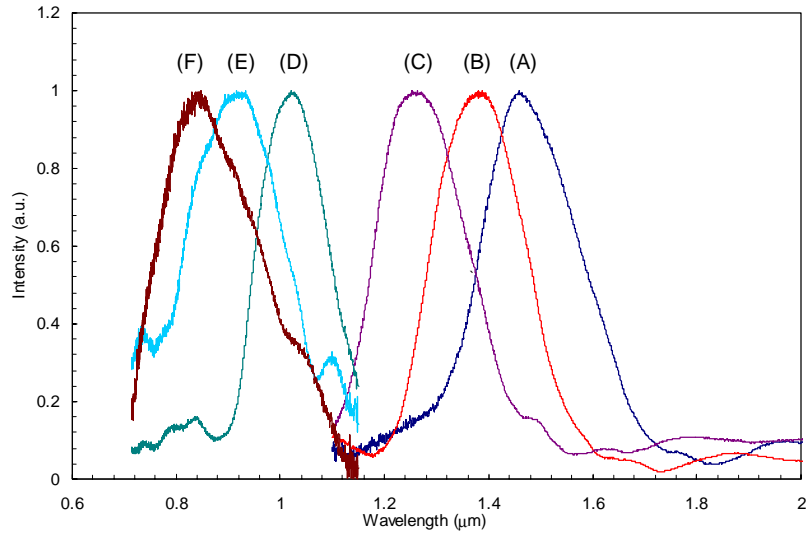


Fig. 4. Measured normalized transmission spectra for (A) 1,218- $\mu\text{m}$ -OD, (B) 1,094- $\mu\text{m}$ -OD, (C) 1,013- $\mu\text{m}$ -OD, (D) 783- $\mu\text{m}$ -OD, (E) 621- $\mu\text{m}$ -OD, (F) 509- $\mu\text{m}$ -OD hollow-core photonic bandgap fibers. The fundamental photonic bandgaps are centered from 0.85 to 1.47  $\mu\text{m}$ . Peak wavelengths from (A) to (F) are 1.47, 1.39, 1.27, 1.03, 1.93 and 0.85  $\mu\text{m}$ , respectively.

As mentioned previously, the spectral positions of the photonic bandgaps were controlled by the laser monitoring of the outer diameter of the fibers during draw. Fibers with an outer diameter of 1.218 and 509  $\mu\text{m}$  have fundamental bandgaps at 1.47 and 0.85  $\mu\text{m}$ , respectively. Fig. 4 shows the wavelength scalability of these fibers, with the comparison of the transmission spectra for six different fibers. These six fibers have fundamental bandgaps centered at 1.47, 1.39, 1.27, 1.03, 0.93 and 0.85  $\mu\text{m}$ , respectively. These wavelengths span a range covering the laser lines of many commercially important lasers, such as Nd:YAG at 1.06  $\mu\text{m}$ , and laser diodes at 0.85  $\mu\text{m}$ . Visible colors from high-order photonic bandgaps in some of these fibers can be seen externally through the cladding of the fibers (Fig. 5).

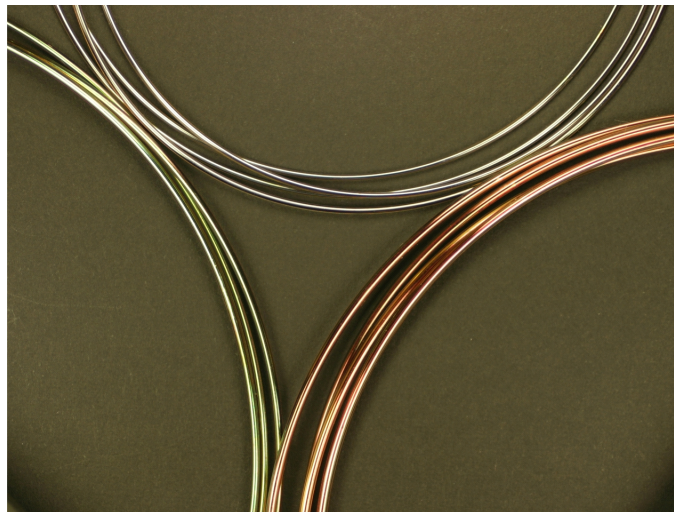


Fig. 5. Coiled fibers made from 1,218- $\mu\text{m}$ -OD (red), 1,013- $\mu\text{m}$ -OD (green), and 621- $\mu\text{m}$ -OD (blue) fibers used to obtain transmission data in Fig. 4.

A critical factor in optical waveguide performance is transmission loss. A fiber cutback measurement was performed with a 5-m fiber having a fundamental bandgap at  $1.57\ \mu\text{m}$ , 26 bilayers and core size of  $165\ \mu\text{m}$ . The fiber was held straight; it was fixed at two points to prevent variations in the input coupling and propagation conditions during the measurement. The laser beam, tuned to  $1.57\ \mu\text{m}$ , was sent through a collimating lens. The transmission loss as measured for the last 2-m section of the fiber was  $\sim 5.5\ \text{dB/m}$ . Radiation losses were measured prior to the cutback by scanning the outer surface of the fiber with a power detector. We found these measured radiation losses to be comparable to the fiber transmission losses, suggesting that the losses are radiation limited.

While for the  $10.6\ \mu\text{m}$  fibers fabricated previously [9], good agreement between cutback measurements and theoretical loss analysis has been obtained, the transmission losses remain high for the near-infrared wavelength fibers reported here compared to loss calculations for an ideal fiber. Fig. 6 inset shows a near-field image of the core intensity as captured during the cutback measurement after 5-m of fiber. We estimate the modal decomposition of the image to be comprised of a superposition of less than the 40 lowest-energy modes. The transmission losses for the 40 lowest energy modes in an flawless structure, is calculated using the leaky mode technique [11] and shown in Fig. 6. The calculated losses for all modes are below  $1\ \text{dB/m}$ , well below the measured fiber transmission losses.

The disparity between the calculated and measured losses may be attributed to the following mechanisms which are not accounted for in our current model: 1) defects such as dust, internal surface roughness, or the formation of crystallites in  $\text{As}_2\text{Se}_3$ ; and 2) non-uniformity in the layer thicknesses introduced from roughness of the initial polymer films, and non-uniform deposition. Improvements in fabrication methods are expected to systematically reduce these loss mechanisms.

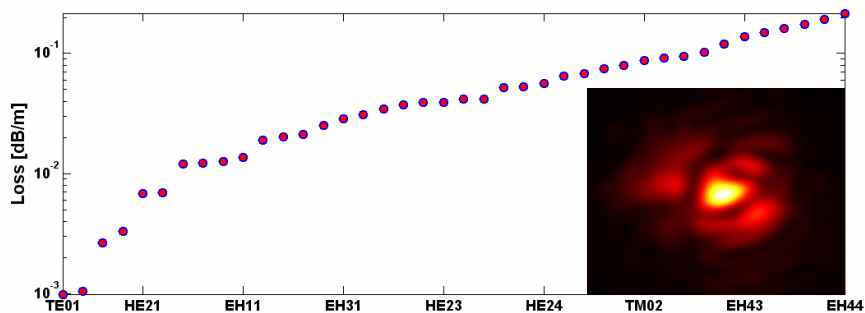


Fig. 6. Loss calculations for the 40 lowest-energy modes in a defect-free cylindrical PBG fiber having the same geometry as the measured fiber. The inset shows a near-field image of the core intensity as taken during the cutback measurement after 5-m of fiber.

#### 4. Conclusion

Nearly-cylindrical photonic bandgap fibers have been fabricated for the first time with fundamental photonic bandgaps at wavelengths ranging from 0.85 to 2.28  $\mu\text{m}$ . These fibers rely on a photonic bandgap to guide light through a hollow core. The photonic bandgaps are created by an all-solid multilayer composite meso-structure having a photonic crystal lattice period as small as 260 nm, individual layers below 75 nm and as many as 35 periods. These represent, to the best of our knowledge, the smallest period lengths and highest period counts reported to date for hollow PBG fibers. The fibers are drawn from a multilayer preform into extended lengths of fiber. We have incorporated a new material into the fiber layer structure, PEI, and compared its optical properties to the previously used  $\text{As}_2\text{Se}_3$  and PES. This work demonstrates the wavelength and small-feature size scalability of the materials and processes employed, as well as the potential for the application of these fibers for short wavelength applications.

#### Acknowledgments

The authors thank Dr. P. Prideaux, M. Frongillo, Dr. A. Abouraddy, and F. Sorin for valuable assistance.

Major funding received from DARPA QuIST Program 6891943 - DAAD19-01-1-0647. This work was also funded in part by: ONR-6893562 - N00014-02-1-0717, AFOSR HEL-MURI - 6893971 - Y77011, the NSF Ultra Hi Capacity - 6892587- ECS-0123460, Deshpande - 6895554 - Internal Sponsor MIT - Innovation Program Grant - MIT Award# 009216-033, the U.S. Army through the Institute for Soldier Nanotechnologies, under Contract DAAD-19-02-D0002, the Materials Research Science and Engineering Center program of the NSF under Grant No. DMR-9400334. This work was also supported in part by the MRSEC Program of the National Science Foundation under award number DMR 02-13282.